INTERNATIONAL JOURNAL OF HYDROGEN ENERGY 39 (2014) 3719–3729

Available online at www.sciencedirect.com

ScienceDirect

journal homepage: www.elsevier.com/locate/he

Preferential CO oxidation on Pt–Cu/Al_2O_3 catalysts with low Pt loadings

Leticia E. Gómez [a], *Brenda M. Sollier* [a], *Martín D. Mizrahi* [b], *José M. Ramallo López* [b], *Eduardo E. Miró* [a], *Alicia V. Boix* [a,*]

[a] *Instituto de Investigaciones en Catálisis y Petroquímica, INCAPE (FIQ, UNL – CONICET), Santiago del Estero 2829, 3000 Santa Fe, Argentina*

[b] *Instituto de Investigaciones Fisicoquímicas Teóricas y Aplicadas, INIFTA (CCT La Plata – CONICET, UNLP), Diagonal 113 y calle 64, 1900 La Plata, Argentina*

ARTICLE INFO

Article history:
Received 23 September 2013
Received in revised form
18 December 2013
Accepted 25 December 2013
Available online 1 February 2014

Keywords:
COPrOx
EXAFS-XANES
Pt–Cu bimetallic
XPS

ABSTRACT

This work demonstrates that a small loading of Pt (0.2–0.5 wt.%) selectively located at the top of the Cu/Al_2O_3 solid is enough to obtain active catalysts for the COPrOx reaction. The characterizations of the catalysts prepared in this work using different Pt:Cu ratios show that the phases formed strongly depend on the Cu and Pt loadings. For the samples with 4 wt.% of Cu, the formation of defective $CuAl_2O_4$-like species is predominant, with Cu^{2+} occupying distorted sites in the alumina surface. For the samples with 8 wt.% of Cu, CuO and metallic Cu in the form of small crystals are observed besides Cu^{2+}. For both 0.2 and 0.5 wt.% of Pt, some proportion of Cu–Pt alloy is found which increased with the Cu content. Metallic Pt particles are only observed by EXAFS for the samples with a higher loading of the noble metal.

The higher CO conversions at low temperatures were obtained for the $Pt_{0.5}Cu_8/Al_2O_3$ sample, probably due to the simultaneous formation of small Pt crystals in close contact with CuO. The XPS results show that a strong surface enrichment in Pt takes place in all the samples. Thus, a small loading of the noble metal is enough to obtain effective catalysts. The surface Pt enrichment observed is most probably due to the impregnation of the Pt salt onto the Cu/Al_2O_3 solid, with a relatively low calcination temperature (300 °C) that prevents the formation of bulky $CuAl_2O_4$ spinel crystals.

1. Introduction

One way to produce the hydrogen to be used in PEM fuel cells is by means of steam reforming or autothermal reforming of hydrocarbons. Generally, this step is followed by the Water Gas Shift (WGS) reaction, where the hydrogen stream is purified. However, the effluent of the WGS reaction contains around 1% CO and it could poison the cell anode. The CO preferential oxidation (COPrOx) is an adequate method to reduce the CO concentration to less than 10 ppm [1]. Thus, given the importance of the hydrogen purification process, the last few years have witnessed the surge of a renewed interest in the CO oxidation reaction, and several contributions dealing with this issue have recently been published. Among

* *Corresponding author*. Tel.: +54 342 4536861.
E-mail address: aboix@fiq.unl.edu.ar (A.V. Boix).

0360-3199/$ – see front matter
http://dx.doi.org/10.1016/j.ijhydene.2013.12.146

the many strategies studied, the preferential oxidation of CO (COPrOx) that selectively oxidizes CO in excess H_2 is an extremely simple and effective method to obtain clean H_2 in a wide operation temperature window (80–180 °C) for the practical application of fuel cells [2].

The prime requirement of a good COPrOx catalyst is high activity and selectivity toward the oxidation of CO rather than toward the oxidation of H_2. Numerous types of catalytic systems such as the noble metal Au [3–5], Pt [4,6] Rh [4], Ru [4,7], Pd [8] supported on different carriers, the bimetallic systems [9,10], and the mixed transition metal oxides of CuOx–CeO_2 [11,12], CoOx–CeO_2 [13,14], CoOx–ZrO_2 [15] and mixed oxides MnCoCeOx [16] have traditionally been studied.

Different methods were used to prepare intermetallic compounds supported on alumina. Komatsu et al. [17] prepared PtCu intermetallic catalysts by the LRD method (3 wt.% Pt and Pt/Cu = 1 atomic ratio), which were more active in COPrOx than Pt–Cu/Al_2O_3 prepared by the usual impregnation method. By in situ FTIR spectroscopy during the PrOx reaction, CO and O_2 are adsorbed preferentially on Pt and Cu atoms, and the formation of CO_2 proceeds through bicarbonate intermediate species with the help of hydroxyl groups of alumina.

To the best of our knowledge, the studies published so far for the COPrOx reaction on Pt–Cu catalysts were performed with relatively high platinum loadings [17–19] (typically between 1 and 3 wt.%). In this work, we explore the performance of catalysts with low Pt loadings, and different Pt:Cu ratios, and we demonstrate that an adequate preparation strategy results in catalysts that have good activity and selectivity with significantly lower amounts of the noble metals.

The catalysts we prepared were carefully characterized by X-ray Diffraction (XRD), X-ray absorption near edge spectroscopy (XANES), X-ray absorption fine structure spectroscopy (EXAFS) and X-ray Photoelectron Spectroscopy (XPS) in order to correlate the catalytic behavior with the physical chemistry properties of the solids.

2. Experimental

2.1. *Preparation of PtCu/Al_2O_3 catalysts*

Four different PtCu/Al_2O_3 bimetallic catalysts were prepared with approximately 4 and 8 wt.% Cu and with 0.2 and 0.5 wt.% Pt, respectively. CuO/Al_2O_3 was synthesized first and, in a second step, the desired amount of Pt was deposited. CuO/Al_2O_3 was prepared by wet impregnation of a powdered alumina support (γ-Al_2O_3, Puralox®, 230 $m^2\ g^{-1}$) with a water solution of $Cu(NO_3)_2 \cdot 3H_2O$ (Merck, p.a.). The mixture was evaporated under continuous stirring at 110 °C until achieving a paste, which was dried in the oven at 120 °C overnight. Subsequently, the sample was calcined in air with a ramping temperature of 5 °C min^{-1} up to 300 °C, where it was kept constant for 3 h. The monometallic CuO/Al_2O_3 samples were labelled Cu_4/Al_2O_3 and Cu_8/Al_2O_3. For the preparation of PtCu/Al_2O_3 catalysts, 6 g of the CuO/Al_2O_3 sample were impregnated with 15 ml of tetraammineplatinum(II) nitrate aqueous solution (Sigma Aldrich) with the appropriate concentration to achieve 0.2 and 0.5 wt.% Pt. In a similar way, the monometallic $Pt_{0.5}/Al_2O_3$ catalyst was prepared by impregnating alumina with a platinum precursor salt. The Pt/Al_2O_3 and PtCu/Al_2O_3 precursors were dried and calcined with the same procedure as that used for CuO/Al_2O_3.

2.2. *Characterization techniques*

2.2.1. *Chemical composition determinations*

Elemental analyses of catalysts were performed by inductively coupled plasma atomic emission spectroscopy (ICP-AES) on an ICP-OPTIMA 2100 DV Perkin Elmer instrument. A summary of the catalysts preparation is shown in Table 1.

2.2.2. *X-ray diffraction (XRD)*

The patterns of catalysts were measured on a Shimadzu XD-D1 with monochromator using Cu-K α radiation at a scanning rate of 1° min^{-1} in $2\theta = 20–80°$. Before the measurements, bimetallic samples were reduced in 20% H_2/He flow at 300 °C (ex situ). The peaks observed for the catalysts were compared to standards published by JCPDS data [20].

2.2.3. *EXAFS/XANES*

2.2.3.1. *X-ray absorption fine structure spectroscopy*. Cu K- and Pt L_3-edges XAFS spectra were measured at room temperature in transmission mode at the XAFS2 beamline at the Laboratorio Nacional de Luz Síncrotron (LNLS, Campinas, Brazil). Powdered samples of the catalysts were pressed in pellets inside an argon glovebox and sealed in cells with kapton windows in order to avoid contact with air. Ionization chambers were used to detect the incident and transmitted flux. Data were processed using ATHENA with the AUTOBK background removal algorithm [21]. The XANES (X-ray Absorption Near Edge Structure) spectra were pre- and postedge normalized to obtain an edge jump of unity to facilitate comparisons across different samples. Spectra were aligned using the corresponding metallic references measured simultaneously with the samples in a third ionization chamber. The EXAFS (Extended X-ray Absorption Fine Structure) oscillations $\chi(k)$ were extracted from the experimental data with standard procedures using the Athena program [21]. The Fourier transformation was calculated using the Hanning filtering function. The k^2 weighted $\chi(k)$ data, to enhance the oscillations at higher k, were Fourier transformed. EXAFS modeling was carried out using the ARTEMIS program which is part of the IFFEFIT package [21,22]. Structural parameters (coordination numbers and bond lengths and their mean squared disorders) were obtained by a nonlinear least-

Table 1 – Chemical composition and catalytic performance of Pt–Cu/Al_2O_3 catalysts.

Catalysts	Pt wt.%	Cu wt.%	CO conversion (%) at 110 °C	Maximum CO conversion	
				(%)	T (°C)
$Pt_{0.2}Cu_4/Al_2O_3$	0.18	3.81	51	92	125
$Pt_{0.2}Cu_8/Al_2O_3$	0.26	7.35	37	87	125
$Pt_{0.5}Cu_4/Al_2O_3$	0.44	3.74	60	97	125
$Pt_{0.5}Cu_8/Al_2O_3$	0.44	8.10	95	99	115
$Pt_{0.5}/Al_2O_3$	0.43	–	13	75	160
Cu_8/Al_2O_3	–	7.53	7	53	175

squares fit of the theoretical EXAFS signal to the data in R space by Fourier transforming both the theory and the data. Theoretical scattering path amplitudes and phase shifts for all paths used in the fits were calculated using the FEFF6 code [23]. The k-range was set from 2 to 14 $Å^{-1}$ and the Fourier transform was fitted in different regions depending on the sample and the edge. The passive reduction factor S_0^2 was restrained to values of 0.91 and 0.93 for Pt L_3 and Cu K-edges analysis, respectively. These values were obtained from fitting of metallic Pt and Cu foils standards by constraining the coordination number in these compounds of known crystalline structure.

2.2.4. *Temperature-programmed reduction (H_2-TPR)*

The reduction under hydrogen was measured with a Micromeritics 2920 instrument. The reducing gas was a 2% H_2/Ar mixture, and the temperature was ramped up at 10 °C min^{-1} to 900 °C. In all cases, a mass of 100 mg was placed in a quartz U-shaped reactor. Prior to the TPR test, the samples were pretreated in Ar at 150 °C for 30 min in order to clean the surface.

2.2.5. *X-ray photoelectron spectroscopy (XPS)*

The surface features of the catalysts were studied in a multitechnique system (SPECS) equipped with a dual Mg/Al X-ray source and a hemispherical PHOIBOS 150 analyzer operating in the fixed analyzer transmission (FAT) mode. The spectra were obtained with a pass energy of 30 eV; the Mg Kα X-ray source was operated at 200 W and 12 kV. The working pressure in the analyzing chamber was less than 5.9×10^{-7} Pa. The XPS analyses were performed on the previously calcined samples, which were in situ reduced inside the reaction chamber of the spectrometer with H_2/Ar flow at 300 °C. The spectral regions corresponding to Cu 2p, Pt 4d, Pt 4f-Al 2p, Al 2s, O 1s core levels were recorded for each sample. The static charge of the samples was corrected by referencing all binding energies (BE) to the C 1s peak (BE = 284.6 eV). The accuracy of the BE was ±0.1 eV. The data treatment was performed with the Casa XPS program (Casa Software Ltda., UK). The areas of the peaks were computed by fitting the experimental spectra to Gaussian/Lorenztian curves after removing the background (using the Shirley function). Surface atom ratios were calculated from peak area ratios normalized by means of the corresponding atomic sensitivity factors.

2.3. *Activity measurements*

Preferential CO oxidation experiments were performed in a fixed-bed flow reactor at atmospheric pressure. Catalysts were placed between quartz glass woods in a quartz reactor (8 mm diameter). In general, the reaction mixture consisted of CO 1%, O_2 1% and H_2 40%, He balance. The catalyst weight/total flow ratio was 2.1 mg cm^{-3} min. The CO conversion and selectivity towards CO_2 were defined as:

$$C_{CO} = \left(\frac{[CO]^0 - [CO]}{[CO]^0}\right) \times 100$$

$$S = \left(\frac{[CO]^0 - [CO]}{[O_2]^0 - [O_2]}\right) \times 100$$

where [CO], $[O_2]$ are reactor exit concentrations and $[CO]^0$, $[O_2]^0$ represent feed concentrations, which were measured with a GC-2014 Shimadzu chromatograph equipped with a TCD cell. All the catalysts were in situ reduced during 2 h in H_2/He flow at 300 °C before the catalytic test.

3. Results and discussion

Table 1 shows a summary of the Pt and Cu loadings for the different formulations prepared.

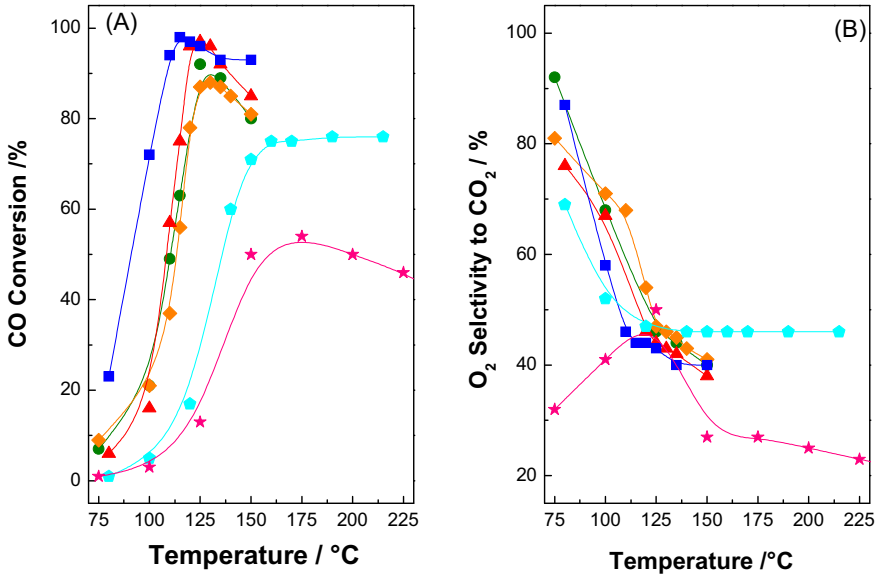

Fig. 1 – COPrOx reaction on $PtCu/Al_2O_3$ catalysts. A: CO Conversion (%). B: O_2 Selectivity to CO_2 (%).● $Pt_{0.2}Cu_4$, ◆ $Pt_{0.2}Cu_8$, ▲ $Pt_{0.5}Cu_4$, ■ $Pt_{0.5}Cu_8$, ⬟ $Pt_{0.5}/Al_2O_3$ and ★ Cu_8/Al_2O_3. Reaction conditions: CO 1%, O_2 1%, H_2 40%, He. W/F: 2.1 mg cm^{-3} min.

The compositions of the samples were analyzed by ICP and they are in agreement with the predefined nominal values.

3.1. Catalytic behavior of the $PtCu/Al_2O_3$ catalysts in the COPrOx reaction

The curves related to CO conversion and selectivity to CO_2 formation corresponding to mono and bimetallic catalysts are shown in Fig. 1. The bimetallic samples were very active for the COPrOx reaction, achieving high conversions of CO at relatively low temperatures. However, the monometallic catalysts $Pt_{0.5}/Al_2O_3$ and Cu_8/Al_2O_3 were significantly less active than the bimetallic catalysts.

The maximum conversions of bimetallic catalysts with lower Pt content, $Pt_{0.2}Cu_4$ and $Pt_{0.2}Cu_8$ were 92 and 87% at 125 °C (Table 1), while the catalysts with 0.5 wt.% Pt reached almost complete CO conversion at 115 °C and 125 °C when the Cu content was 8 and 4 wt.%, respectively. The catalytic behavior shows that a slightly increase of Pt concentration (0.2–0.5 wt.%) notably improves the CO conversion at low temperature. In all cases, the selectivity curves showed a declining trend with increasing temperature. Unlike these curves, the selectivity of Cu_8/Al_2O_3 catalyst showed a maximum at 80 °C. The better performance of bimetallic catalysts compared to that of monometallic ones might indicate that a synergic effect between Pt and Cu exists and promotes the CO oxidation.

Our results are in line with recently reported data in the literature. These PtCu systems were prepared by various methods with Pt loadings higher than 1 wt.% and were evaluated under different COPrOx reaction conditions. Kugai et al. [19] evaluated $PtCu/Al_2O_3$ (2.45 wt.% Pt, 0.13 wt.% Cu) prepared by electron beam irradiation method and reached a maximum of 50% CO conversion at 120 °C, with a higher concentration of H_2 (62%) in the stream. In addition, they observed a better catalytic behavior with 10% of water in the feed. Mozer and Passos [18] also obtained a relatively low conversion (40%) at 350 °C with 1%Pt–1%Cu/Al_2O_3 prepared by the incipient wetness technique, in the presence of 30% CO_2 and 10% H_2O. Additional studies are ongoing to assess the effect of water and CO_2 on the activity and selectivity of our catalysts. Komatsu et al. [17] prepared Pt–Cu/Al_2O_3 catalysts by the co-impregnation method and liquid-phase reductive deposition (LRD) with 3 wt.% Pt and atomic ratio Pt/Cu = 1. The best catalyst, prepared by the LRD method, showed 98% of CO conversion at 80 °C. While the co-impregnated catalyst presented a lower CO conversion, 85% at 180 °C. Different platinum bimetallic systems were reported as active and selective catalysts in the COPrOx reaction. However, not always was the complete CO conversion at low temperature achieved.

In order to compare with values reported in the literature for similar catalysts, we have considered to estimate the value of TOF, on the basis of moles of hydrogen chemisorbed on Pt sites, assuming a stoichiometry of H:Pt = 1:1. The moles of hydrogen (H) irreversibly chemisorbed on the $Pt_{0.5}Cu_8/Al_2O_3$ catalyst were 4.56 10^{-6} mol g^{-1}, whereby the TOF ~ 0.2 s^{-1} at 80° C. This value is within the same order of magnitude as the value reported by Komatsu and Tamura [24] for $PtCu/SiO_2$ catalyst, measured at 80° C.

3.2. Characterization of $PtCu/Al_2O_3$ catalysts

Fig. 2 shows the XRD patterns of the $PtCu/Al_2O_3$ catalysts calcined and reduced at 300 °C, which were recorded in order to identify the crystalline phases formed before the catalytic test. The diffractogram obtained with the calcined Al_2O_3 support is also shown.

The XRD patterns of $PtCu/Al_2O_3$ with 8 wt.% Cu show the presence of CuO on the calcined samples with the main lines at 2θ = 35.5 and 38.7°(JCPDS 44-706). After reducing the catalysts, the diffraction peaks corresponding to metallic Cu crystallites at 2θ = 43.3, 50.5 and 74.2° (JCPDS 4-836) can be observed. The average particle sizes were estimated from the main peaks using Scherrer's equation, which resulted 12–13 nm for CuO particles and 15–17 nm for metallic Cu ones. On the other hand, no diffraction line corresponding to platinum species or bimetallic Pt–Cu alloy particles are detected. For the bimetallic catalysts with 4 wt.% Cu, CuO or Cu(0) crystallites are not observed, which would suggest that copper is highly dispersed on the support, although the overlap of the corresponding diffraction lines of CuO or Cu(0) and Al_2O_3 (2θ = 37.6, 39.5, 45.9 and 67.1°, JCDPS10-425) cannot be discarded.

Fig. 3 shows the XANES results at the Cu K-edge of the different catalysts compared with those of CuO, Cu_2O and

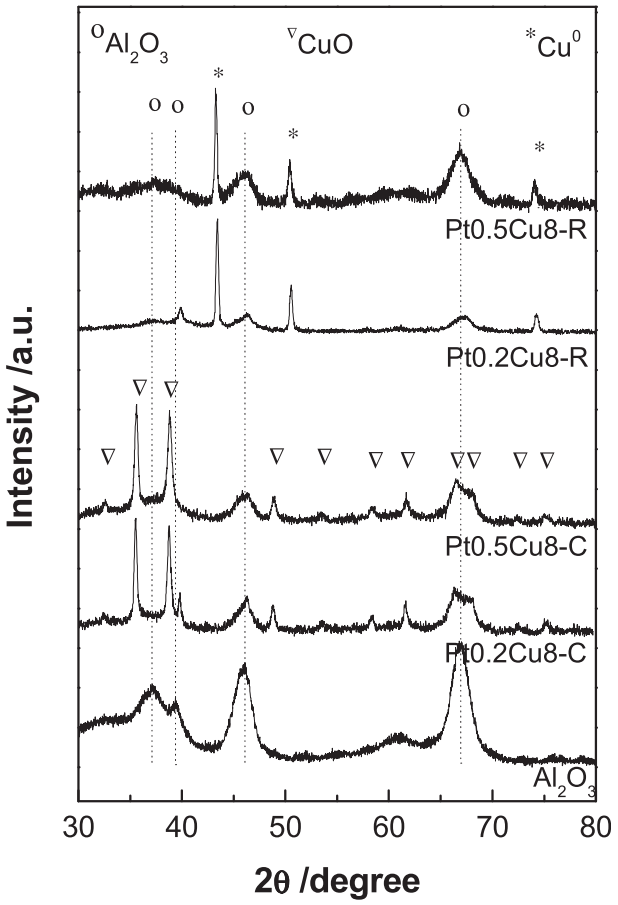

Fig. 2 – X ray diffraction patterns of Al_2O_3 support and $Pt_{0.5}Cu_8/Al_2O_3$ and $Pt_{0.2}Cu_8/Al_2O_3$ catalysts calcined (C) and reduced (R).

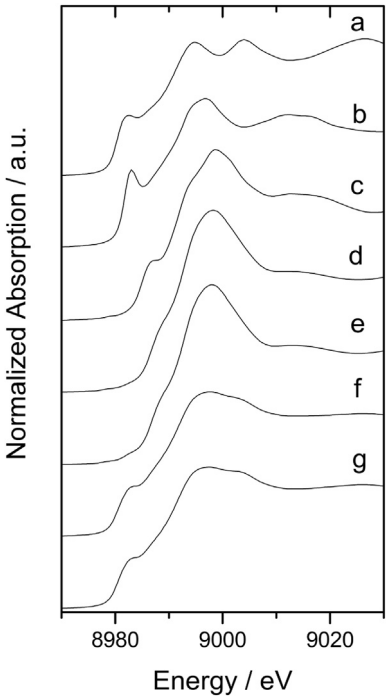

Fig. 3 – XANES spectra at the Cu K-edge: a) Cu foil, b) Cu_2O, c) CuO, d) $Pt_{0.2}Cu_4/Al_2O_3$ e) $Pt_{0.5}Cu_4/Al_2O_3$, f) $Pt_{0.2}Cu_8/Al_2O_3$, g) $Pt_{0.5}Cu_8/Al_2O_3$.

metallic Cu. The XANES spectra can be seen as a fingerprint of the compound and their different features can be used to obtain information of the oxidation state and the local structure of copper atoms. For metallic copper, the signal at 8982 eV is assigned to a 1s → 4p transition. A small pre-edge peak is found for CuO at 8978 eV which is assigned to the dipole-forbidden electronic transition of 1s → 3d [25]. Its presence is characteristic of a distorted octahedral coordination. The more intense peaks observed at 8983 and 8987 eV for Cu_2O and for CuO, respectively are attributed to the dipole-allowed 1s → 4p electron transition [26]. The position of the absorption edge can be related to the oxidation state of the absorbing atom. As the oxidation state is higher, the edge is shifted to higher energies as it can be seen in Fig. 3 for the three reference compounds [27]. Considering the edge position, XANES results show that in the bimetallic catalysts with 4 wt.% Cu, Cu atoms are present as Cu^{2+}.

When analyzing the different species reported for Cu/Al_2O_3, well-dispersed isolated Cu^{2+} as well as a copper surface spinel have been observed [28,29]. The latter is a defective $CuAl_2O_4$-like species, with Cu^{2+} occupying distorted sites on the alumina surface [30]. Bulk CuO starts to appear [28] only with loadings over 10 wt.% Cu. The possibility of filling surface defect sites of alumina with copper ions to form a $CuAl_2O_4$ surface spinel-type compound was first shown by Wolberg and Roth [31] in their early X-ray absorption spectroscopy study of Cu/Al_2O_3. Shimizu et al. [32] showed that the white line of bulk $CuAl_2O_4$ has three well defined peaks at 8996, 8999 and 9003 eV, and when the loading of Cu in Cu/Al_2O_3 is decreased, these features are softened and become unresolved below 8 wt.% Cu loading while the pre-edge peak at 8979 eV decreases its intensity. Our catalysts with the lower Cu loading have similar XANES features. This indicates that the local structure of Cu^{2+} species in the catalysts is different from the bulk CuO because of the interaction with the support, probably forming the reported surface spinel-type species. Samples with 8 wt.% Cu loading show differences in their XANES spectra with respect to those with a lower loading, with a shift in the absorption edge position to lower energy and more similarities to the XANES spectrum of metallic Cu. As said above, it has been shown that the loadings of 10 wt.% Cu lead to the formation of CuO which can be reduced to metallic Cu. In our catalysts, XANES results would indicate that part of the Cu atoms are now as Cu(0), while the other fractions may still remain as Cu^{2+}, forming the same structures as in the lower Cu loading catalysts.

Fig. 4 shows the magnitude of the Fourier transformed EXAFS signals obtained at both edges for the catalysts compared with reference compounds. No phase correction was applied to the Fourier transforms; consequently, the *R* distance where each peak appears does not correspond to the real interatomic distance, but the Fourier transforms can be used for comparison with the references. At the Cu K-edge, the presence of a Cu–O shell (at 1.4 Å) is found in the samples with 4 wt.% Cu. However, no further coordination shells are present in these catalysts, indicating that the species correspond to diluted and isolated oxide species, in agreement with XANES results. Two shells, a Cu–O shell and a Cu–Cu (at 2.2 Å) one, are observed for the samples with 8 wt.% Cu, indicating the co-existence of an oxide and a metallic species, in agreement with XANES results.

When analyzing the Pt L_3 edge, both Pt–O and metallic shells are observed in all samples.

The EXAFS analysis was performed in the R-space using the Arthemis program [21]. EXAFS signals at the Cu K-edge were fitted proposing Cu–O and Cu–Cu shells. For the Pt L_3-edge results, a two-shell model was not enough to fit all samples and we had to propose a three-shell model: Pt–O, Pt–Pt and Pt–Cu shells.

Fitted functions and their corresponding parameters for the EXAFS signals obtained at the Cu K-edge are shown in Fig. 5 and Table 2. When analyzing the Cu K-edge, we found similar results for samples with the same quantity of Cu. For the samples with 4 wt.% of Cu, we only found an oxygen shell with an average coordination number (ACN) N_{Cu-O} between 3 and 4. This shows that almost all Cu is present in oxidized species in agreement with XANES results. For the samples with 8 wt.% of Cu, we obtained smaller values for N_{Cu-O} (around 1.5) and a new Cu shell with ACN N_{Cu-Cu} around 4. In these cases, a proportion of Cu atoms are in metallic state. If we assume that the oxidized species are the same as in the samples with 4 wt.% of Cu, the ACN N_{Cu-O} fitted is smaller because it is weighted by the fraction of those species in the sample; thus, a bit less than 50% of Cu atoms would be forming those species. The rest of the Cu atoms are in metallic state, probably forming small particles, as the ACN normalized by the fraction of that species would be between 8 and 9, and still smaller than the value of the bulk (12).

Fig. 6 and Table 3 show the results obtained from the fits of the Pt L_3 edge EXAFS results. Catalysts with the lower Pt loading have two shells around Pt, one of oxygen and one of

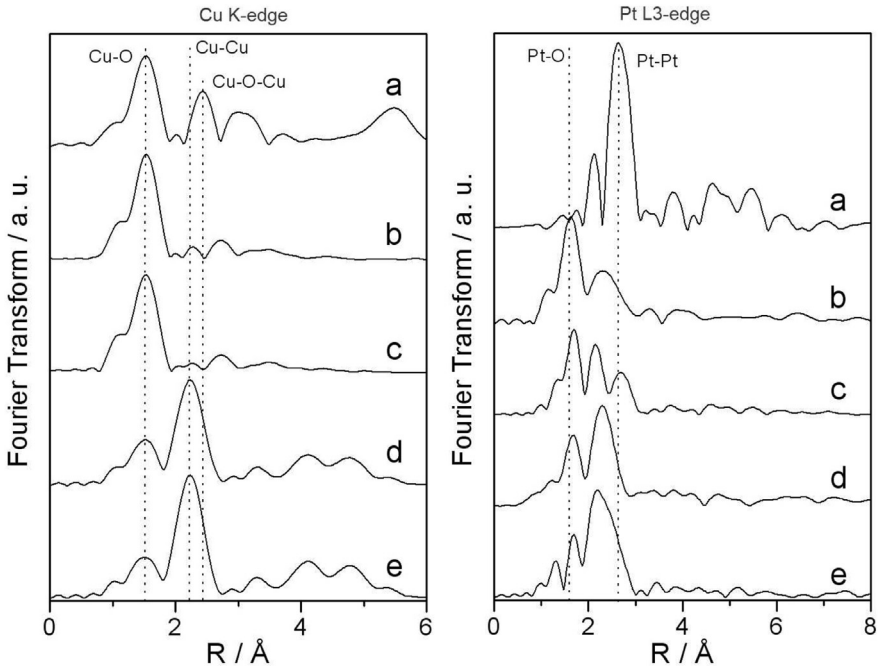

Fig. 4 – Magnitude of the Fourier transforms of the EXAFS signals obtained at the Cu K edge (left) and Pt L_3 edge (right). a) Reference compounds (left: CuO, right: metallic Pt), b) $Pt_{0.2}Cu_4/Al_2O_3$ c) $Pt_{0.5}Cu_4/Al_2O_3$, d) $Pt_{0.2}Cu_8/Al_2O_3$, e) $Pt_{0.5}Cu_8/Al_2O_3$.

copper atoms, indicating the presence of a fraction of Pt oxide and a fraction of Pt–Cu alloy. The fraction of alloy increases when the Cu loading is higher. When the Pt loading is 0.5 wt.%, a new Pt–Pt shell is found indicating that a fraction of Pt atoms are segregated forming metallic Pt, in addition to the oxide and the alloy. For these catalysts, it is also observed that the fraction of alloy increases when the loading of Cu is higher. The absence of a Cu–Pt shell in the Cu K-edge EXAFS results can be understood in terms of the atomic relation Cu/Pt in the catalysts. As the amount of Cu atoms in all catalyst is considerably higher in all cases and only a small fraction of them are forming the alloy, the average coordination number that would result for the Cu–Pt shell would be too small to be detected from the EXAFS analysis.

In brief, the results obtained at this point with the XRD, EXAFS and XANES techniques show that the bimetallic catalysts are composed of a complex mixture of phases. For the samples with lower Cu loading, the formation of defective $CuAl_2O_4$-like species, with Cu^{2+} occupying distorted sites in the alumina surface, is indicated by EXAFS and XANES results. CuO does not develop in this sample thus not forming metallic clusters after reduction. Differently, for the samples with 8 wt.% Cu, CuO and metallic Cu are observed besides Cu^{2+}. In all samples, some Cu–Pt interactions are found that increase with the Cu content. In line with these results, XRD patterns show the formation of CuO and metallic Cu crystals of about 12–13 nm and 15–17 nm, respectively, only for the samples with higher Cu loading. As regards the formation of metallic Pt crystals, this is observed only for the samples with higher loadings of the noble metal.

Fig. 7 shows the reduction profiles of monometallic samples $Cu4/Al_2O_3$ and $Cu8/Al_2O_3$ and bimetallic catalysts. The profile of $Cu4/Al_2O_3$ shows only one peak at 248 °C, which corresponds to the reduction of CuO. When the amount of Cu is higher, two peaks of reduction are observed, one of them at 276 °C and the other at 311 °C, which are related to two particle sizes [33].

When the bimetallic samples are analyzed, it can be observed that the reduction in all catalysts is produced at lower temperature than in the monometallic samples, and in one stage. In the catalysts with lower Cu content, the maxima are between 234 and 240 °C, and when the Cu content is 8 wt.%, the peaks are around 265–270 °C. Also, a shoulder around 200 °C is observed in the profile of all bimetallic catalysts and it was attributed to PtO_2 reduction, which was also corroborated by the hydrogen consumption.

These results indicate that before the catalytic reaction, all metallic species are completely reduced. Moreover, the presence of the $CuAl_2O_4$ spinel was not detected with the reduction experiment, possibly due to the relatively lower calcination temperature of the catalysts.

In this regard, other authors exhibited similar results. For example, Vila et al. [33] reported that the TPR profiles of the 10 wt.% Cu/Al_2O_3 samples displayed a major H_2 consumption peak with a maximum at 457 K and a shoulder at ca. 500 K. The first peak was attributed to the reduction to metallic copper of the Cu^{2+} species present in well-dispersed CuO particles, whereas the shoulder was related to the reduction of Cu^{2+} in larger CuO particles. Additionally, a small H_2 consumption peak was observed at significant higher temperatures (ca. 721 K), which could be attributed to the reduction of $CuAl_2O_4$ spinel species that were formed during the calcination step.

In the same vein, Mozer and Passos [18] showed a peak at 250 °C and a shoulder at 340 °C in the TPR profile for 1%Pt/

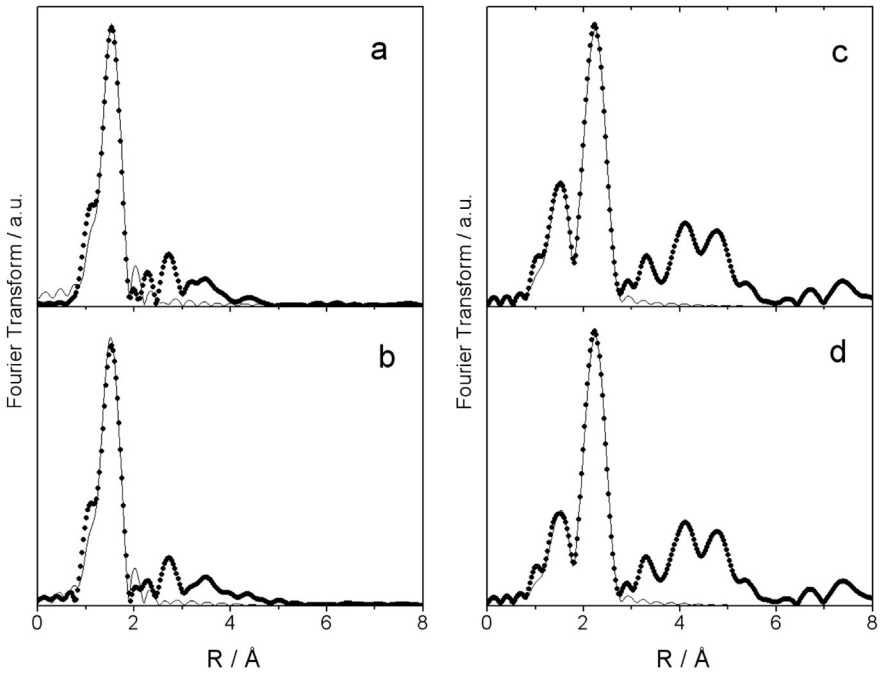

Fig. 5 – Magnitude of the Fourier transforms of the Cu K edge EXAFS signals (solid points) and their corresponding best fits (solid line). a) $Pt_{0.2}Cu_4/Al_2O_3$, b) $Pt_{0.5}Cu_4/Al_2O_3$, c) $Pt_{0.2}Cu_8/Al_2O_3$, d) $Pt_{0.5}Cu_8/Al_2O_3$.

Al_2O_3 catalyst. The TPR profile for 1%Cu/Al_2O_3 showed H_2 uptakes at 290 °C and 385 °C, the former peak due to the partial reduction of Cu^{2+} species present in highly dispersed copper oxide species, while the latter was ascribed to the reduction of Cu^+ species to metallic copper. The bimetallic catalysts showed a peak at 280 °C attributed to the reduction of Pt–Cu oxidized species where both metals were in close contact and the H_2 uptake in the 300–500 °C range corresponded to the reduction of oxidized copper species not interacting with Pt.

It is clear that, comparing the samples $Pt_{0.2}Cu_8/Al_2O_3$ with $Pt_{0.5}Cu_8/Al_2O_3$ it would be expected a higher CO conversion for the second one due to the higher amount of Pt loading that most probably contributes to the formation of more Pt–Cu alloy crystals.

Moreover, by correlating the characterization results described above with the measured catalytic activities, it can be speculated that the CO conversion is improved by the presence of Pt–Cu interactions and/or the formation of CuO and metallic Cu species. These characteristics are more evident in $Pt_{0.5}Cu_8/Al_2O_3$ which is, of all the catalysts here studied, the only catalyst that reached almost complete CO conversion at 115 °C. Another important characteristic of this catalyst is the formation of metallic platinum clusters that are not observed for the samples with 0.2 wt.% of Pt.

The performance of the bimetallic catalysts improves with platinum loading, but is slightly modified with the Cu content. As in the case of catalysts with a low content of Pt (0.2 wt.%), the CO conversion does not change with the increase of Cu loading. In addition, the increase of Pt loading promotes the formation of Pt–Cu alloy crystals and the growth of metallic Pt crystals which are in contact with CuO species.

The surface interaction that could take place in the reaction mechanism consists of the CO adsorption on the Pt sites and the subsequent oxidation of these species by the oxygen atoms associated with Cu, which is a generally accepted redox bi-functional mechanism [34]. The improvement in catalytic activity observed after the addition of the Pt to Cu/Al_2O_3 catalyst could be explained by taking into account that the noble metal provides sites for CO adsorption, and the adsorption is followed by the oxidation from the oxygen atoms associated with Cu particles. Although a competition for CO and H_2 adsorption exists, at low temperature the CO adsorption prevails, thus the selectivity is higher [34]. On the other hand, at elevated temperatures, hydrogen adsorption readily occurs, giving place to lower selectivities. The improved CO conversion for the $Pt_{0.5}Cu_8/Al_2O_3$ sample could also be interpreted in terms of the simultaneous formation of small Pt crystals in close contact with CuO, the first species favoring CO adsorption, which is in turn oxidized with the oxygen associated with CuO. Probably, samples with lower amounts of Cu are less active because Cu is only in the form of $CuAl_2O_4$-like species, which are less reducible as compared to CuO. In the same vein, catalysts with lower Pt loading could be

Table 2 – Results obtained for the fits of the Cu K-edge EXAFS.

Catalyst	Pair	N	R/Å	σ^2/Å^2
$Pt_{0.2}Cu_4/Al_2O_3$	Cu–O	3.5(7)	1.93(2)	0.005(2)
$Pt_{0.5}Cu_4/Al_2O_3$	Cu–O	3.3(6)	1.92(2)	0.005(2)
$Pt_{0.2}Cu_8/Al_2O_3$	Cu–O	1.4(2)	1.91(1)	0.005(2)
	Cu–Cu	4.0(4)	2.54(1)	0.009(1)
$Pt_{0.5}Cu_8/Al_2O_3$	Cu–O	1.3(1)	1.91(1)	0.005(2)
	Cu–Cu	4.6(4)	2.54(1)	0.009(1)

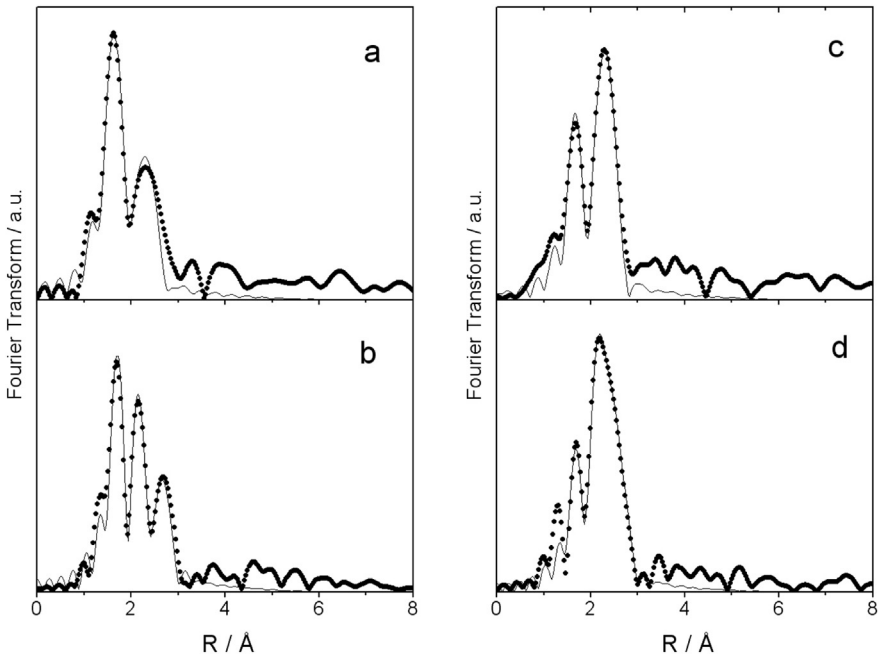

Fig. 6 – Magnitude of the Fourier transforms of the Pt L_3 edge EXAFS signals (solid points) and their corresponding best fits (solid line). a) $Pt_{0.2}Cu_4/Al_2O_3$, b) $Pt_{0.5}Cu_4/Al_2O_3$, c) $Pt_{0.2}Cu_8/Al_2O_3$, d) $Pt_{0.5}Cu_8/Al_2O_3$.

less active due to the formation of isolated Pt species instead of metallic crystals. However, at this point, it is necessary to inspect the surface chemistry of the catalysts in order to better correlate their physical chemistry properties with the catalytic performance.

X-ray photoelectron spectra of the different $PtCu/Al_2O_3$ catalysts were measured with the aim of identifying the oxidation state and estimating the dispersion of copper and platinum species. First, let us note a known problem in the XPS study of Pt/Al_2O_3 catalysts. The Al 2p line of the support overlaps with the Pt 4f line of the active component usually used for the spectroscopic analysis of platinum. This makes the direct analysis of the platinum states very complicated. Therefore, in this study we used a different line, Pt 4d. Although this line is weaker, the peak is not overlapped by the spectral lines of the other components. Fig. 8 presents the spectral region of Pt $4d_{5/2}$ and Cu 2p binding energies of $PtCu/Al_2O_3$ in situ reduced at 300 °C, with subtraction of the background spectrum from scattered electrons approximated using Shirley's method [35]. The decomposition of the spectra to individual components of Pt $4d_{5/2}$ core-level revealed the presence of three different platinum species in the bimetallic catalysts. The main peak component with BE ($Pt4d_{5/2}$) around of 314.7–315.2 eV is assigned to Pt(0) state and the oxidized platinum (Pt–O) with BEs 318.2–318.9 eV [36]. The third peak centered at 312.5–312.6 eV corresponds to Pt(0) belonging to the Pt–Cu alloy or to the intermetallic compound. For comparison purposes, the Pt 4 $d_{5/2}$ spectrum of the $Pt_{0.5}/Al_2O_3$ catalyst reduced in situ at 300 °C has been added to Fig. 8(A). It is possible to distinguish only two components, at 314.0 and 317.1 eV, which correspond to PtOx and Pt(0) species.

On the other hand, the $PtCu/Al_2O_3$ samples, in situ reduced at 300 °C, show a main Cu $2p_{3/2}$ peak at ca. 931.6 eV, which is attributed to Cu(0) species and the corresponding spin orbit splitting Cu $2p_{5/2}$ peak at 951.5 eV. A slight asymmetry observed on the left side of the peak suggests another component in lower concentration, which could be assigned to Cu^+ species. This is further supported by the absence of a satellite peak at higher binding energy (942–943 eV), typical of Cu^{2+} species [33]. It is important to note that the shift to lower binding energies of reduced Cu supported on alumina compared to metallic Cu foil (reported at c.a. 932.5 eV) suggests a strong interaction between Cu particles with alumina surface.

Surface Pt/Al and Cu/Al atomic ratios included in Table 4 were calculated from XPS, taking into account the peak area of the Al 2s region, to avoid overlapping the Al 2p-Pt 4f region.

In the case of bimetallic samples with 4 wt.% Cu, the measured Cu/Al atomic ratios are 0.024–0.026 slightly lower than the nominal ratios (0.033–0.031), which suggests a high dispersion of copper particles on the alumina surface. However, in the catalysts with high Cu content (8 wt.%), the Cu/Al

Table 3 – Results obtained for the fits of the Pt L_3-edge EXAFS.

Catalyst	Pair	N	R/Å	σ^2/Å^2
$Pt_{0.2}Cu_4/Al_2O_3$	Pt–O	2.2(3)	2.10(1)	0.0018(7)
	Pt–Cu	2.5(7)	2.56(2)	0.010(5)
$Pt_{0.2}Cu_8/Al_2O_3$	Pt–O	1.1(3)	2.10(1)	0.0010(5)
	Pt–Cu	3.7(6)	2.58(2)	0.010(5)
$Pt_{0.5}Cu_4/Al_2O_3$	Pt–O	1.1(2)	2.10(1)	0.0010(5)
	Pt–Cu	2.3(6)	2.53(2)	0.010(5)
	Pt–Pt	1.9(5)	2.72(2)	0.007(1)
$Pt_{0.5}Cu_8/Al_2O_3$	Pt–O	0.7(1)	2.10(1)	0.0010(5)
	Pt–Cu	3.7(7)	2.57(2)	0.010(5)
	Pt–Pt	1.7(7)	2.69(2)	0.006(1)

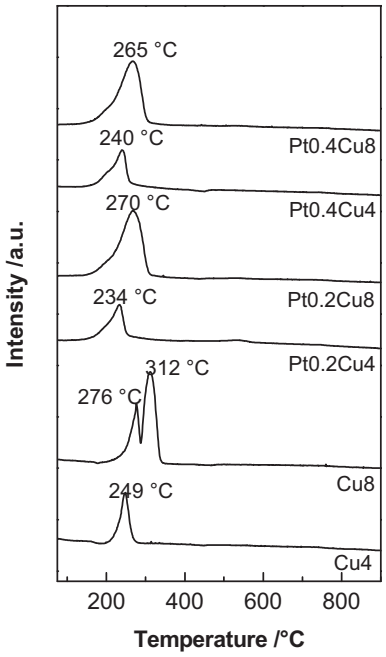

Fig. 7 – TPR profiles of Cu_4/Al_2O_3, Cu_8/Al_2O_3 and bimetallic $PtCu/Al_2O_3$ catalysts.

ratio slightly increases on the alumina surface, which suggests a lower dispersion of copper due to the formation of larger particles according to the diffraction lines of Cu(0) observed. In addition, the platinum surface enrichment can also be observed.

XPS results are in line with the conclusions reached above with EXAFS, XANES and XRD. However, very important new information is revealed, which is the strong surface enrichment in Pt observed for all the samples. In fact, it can be observed that in all cases the surface Pt/Cu ratio is one order of magnitude higher, or more, as compared with the Pt/Cu bulk ratio. Another interesting observation that can be made is that the said surface ratio almost does not change for the different metallic loadings. These results allow us to conclude that, since Pt atoms are preferentially located on the surface of the catalysts, a small loading of the noble metal is enough to obtain effective catalysts. The surface Pt enrichment observed is most probably due to the preparation strategy followed, in which we combined the impregnation of the Pt salt onto the Cu/Al_2O_3 solid, with a relatively low calcination temperature (300 °C). This method favors the Pt–Cu interactions with Pt atoms preferentially exposed to the reactants and prevents the formation of bulky $CuAl_2O_4$ spinel crystals.

4. Conclusions

The bimetallic catalysts prepared in this work are composed of a complex mixture of phases that strongly depend on the Cu and Pt loadings. For the samples with 4 wt.% of Cu, the formation of defective $CuAl_2O_4$-like species is predominant, with Cu^{2+} occupying distorted sites on the alumina surface. For the samples with 8 wt.% of Cu, CuO and metallic Cu in the form of small crystals are observed besides Cu^{2+}. For both 0.2 and 0.5 wt.% of Pt, some Cu–Pt interactions, probably due to

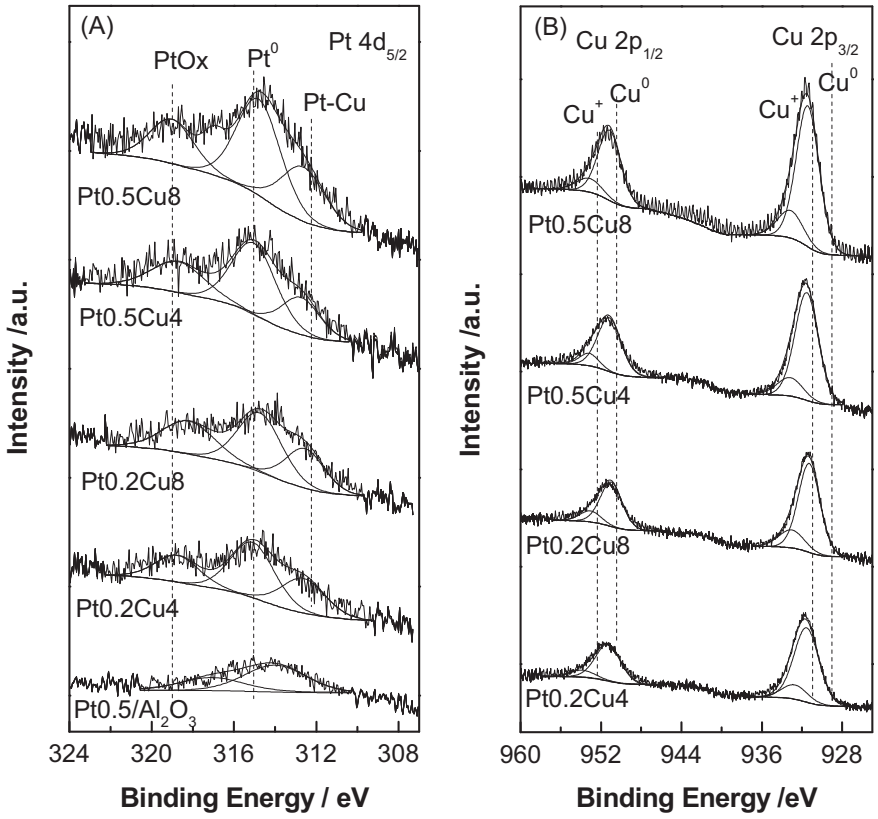

Fig. 8 – XPS spectra of $PtCu/Al_2O_3$ catalysts in situ reduced by H_2/Ar flow at 300 °C. (A) Pt $4d_{5/2}$ region and (B) Cu 2p region.

Table 4 – Summary of XPS. Pt $4d_{5/2}$ and Cu $2p_{3/2}$ binding energy and surface atomic ratio.

Catalysts	Binding energy (eV)[a]		Surface atomic ratio		
	Pt $4d_{5/2}$	Cu $2p_{3/2}$	Pt/Cu	Pt/Al × 10^3	Cu/Al × 10^2
$Pt_{0.2}Cu_4$	312.6 (30) 315.1 (47) 318.7	931.5 (83) 932.8	0.206 [0.015][b]	4.9 [0.48]	2.4 [3.3]
$Pt_{0.2}Cu_8$	312.5 (26) 314.7 (44) 318.2	931.3 (81) 933.0	0.218 [0.011]	6.1 [0.73]	2.8 [6.4]
$Pt_{0.5}Cu_4$	312.7 (23) 315.0 (51) 318.7	931.5 (84) 933.1	0.185 [0.039]	4.9 [1.2]	2.6[3.1]
$Pt_{0.5}Cu_8$	312.6 (26) 314.8 (53) 318.9	931.4 (82) 933.2	0.208 [0.019]	7.0[1.3]	3.3 [6.9]
$Pt_{0.5}/Al_2O_3$	314.0(69) 317.1	–	–	1.5 [2.6]	–

[a] Values between parentheses indicate the percentage.
[b] Values between square brackets indicate bulk atomic ratio.

the presence of alloys, are found and their presence increases with the Cu content. Metallic Pt crystals are only observed by EXAFS for the samples with higher loadings of the noble metal.

The catalytic experiments suggest that the CO conversion is improved by the presence of Pt–Cu interactions and/or the formation of CuO and metallic Cu species, characteristics that are more evident for the $Pt_{0.5}Cu_8/Al_2O_3$ catalyst, which is the most active formulation. The formation of metallic platinum clusters in this solid could also play a role in its improved performance. Thus, the higher CO conversion for the $Pt_{0.5}Cu_8/Al_2O_3$ sample could be interpreted in terms of the simultaneous formation of small Pt crystals in close contact with CuO, the first species favoring CO adsorption, which is in turn oxidized with the oxygen associated with CuO. Probably, samples with a lower amount of Cu are less active because Cu is only in the form of $CuAl_2O_4$-like species, which are less reducible as compared to CuO. In the same vein, catalysts with lower Pt loading could be less active due to the formation of isolated Pt species instead of metallic crystals. The XPS results show a strong surface enrichment in Pt for all the samples. Thus, a small loading of the noble metal is enough to obtain effective catalysts. The surface Pt enrichment observed is most probably due to the impregnation of the Pt salt onto the Cu/Al_2O_3 solid, with a relatively low calcination temperature (300 °C) that prevents the formation of bulky $CuAl_2O_4$ spinel crystals.

Acknowledgments

The authors acknowledge the financial support received from UNL, CONICET, and LNLS (Brasil, Proyect XAFS1 – 12539). They are grateful to ANPCyT for the purchase of the SPECS multitechnique analysis instrument (PME 8-2003) and the TPD/TPR/TPO system (PME-2007-071). Thanks are given to Fernanda Mori for the XPS measurements, to Norma Amadeo for the TPR measurements and to Elsa Grimaldi for the English language editing.

REFERENCES

[1] Bion N, Epron F, Moreno M, Mariño F, Duprez D. Preferential oxidation of carbon monoxide in the presence of hydrogen (PROX) over noble metals and transition metal oxides: advantages and drawbacks. Top Catal 2008;51:76–88.
[2] Park ED, Lee D, Lee HC. Recent progress in selective CO removal in a H_2-rich stream. Catal Today 2009;139:280–90.
[3] Landon P, Ferguson J, Solsona BE, Garcia T, Carley AF, Herzing AA, et al. Selective oxidation of CO in the presence of H_2, H_2O and CO_2 via gold for use in fuel cells. Chem Commun 2005:3385–7.
[4] Kipnis M, Volnina E. New approaches to preferential CO oxidation over noble metals. Appl Catal B Environ 2010;98:193–203.
[5] Kipnis M, Volnina E. H_2 oxidation and preferential CO oxidation over Au: new approaches. Appl Catal B Environ 2011;103:39–47.
[6] Ayastuy JL, González-Marcos MP, Gil-Rodríguez A, González-Velasco JR, Gutiérrez-Ortiz MA. Selective CO oxidation over $Ce_xZr_{1-x}O_2$-supported Pt catalysts. Catal Today 2006;116:391–9.
[7] Kim YH, Park JE, Lee HC, Choi SH, Park ED. Active size-controlled Ru catalysts for selective CO oxidation in H_2. Appl Catal B Environ 2012;127:129–36.
[8] Miguel-García I, Berenguer-Murcia A, Cazorla-Amorós D. Preferential oxidation of CO catalyzed by supported polymer-protected palladium-based nanoparticles. Appl Catal B Environ 2010;98:161–70.
[9] Li D, Liu X, Zhang Q, Wang Y, Wan H. Cobalt and copper composite oxides as efficient catalysts for preferential oxidation of CO in H_2-rich stream. Catal Lett 2009;127:377–85.
[10] Liao X, Chu W, Dai X, Pitchon V. Bimetallic Au-Cu supported on ceria for PROX reaction: effects of Cu/Au atomic ratios and thermal pretreatments. Appl Catal B Environ 2013;142–143:25–37.
[11] Mariño F, Baronetti G, Laborde M, Bion N, Le Valant A, Epron F, et al. Optimized CuO-CeO_2 catalysts for COPROX reaction. Int J Hydrogen Energy 2008;33:1345–53.
[12] Martínez-Arias A, Gamarra D, Fernández-García M, Wang XQ, Hanson JC, Rodriguez JA. Comparative study on redox properties of nanosized CeO_2 and CuO/CeO_2 under CO/O_2. J Catal 2006;240:1–7.

[13] Gómez LE, Tiscornia IS, Boix AV, Miró EE. CO preferential oxidation on cordierite monoliths coated with Co/CeO_2 catalysts. Int J Hydrogen Energy 2012;37:14812–9.
[14] Woods MP, Gawade P, Tan B, Ozkan US. Preferential oxidation of carbon monoxide on Co/CeO_2 nanoparticles. Appl Catal B Environ 2010;97:28–35.
[15] Gomez LE, Tiscornia IS, Boix AV, Miró EE. Co/ZrO_2 catalysts coated on cordierite monoliths for CO preferential oxidation. Appl Catal A Gen 2011;401:124–33.
[16] Gómez LE, Miro EE, Boix AV. Spectroscopic characterization of Mn-Co-Ce mixed oxides, active catalysts for COPROX reaction. Int J Hydrogen Energy 2013;38:5645–54.
[17] Komatsu T, Takasaki M, Ozawa K, Furukawa S, Muramatsu A. PtCu intermetallic compound supported on alumina active for preferential oxidation of CO in hydrogen. J Phys Chem C 2013;117:10483–91.
[18] Mozer TS, Passos FB. Selective CO oxidation on Cu promoted Pt/Al_2O_3 and Pt/Nb_2O_5 catalysts. Int J Hydrogen Energy 2011;36:13369–78.
[19] Kugai J, Moriya T, Seino S, Nakagawa T, Ohkubo Y, Nitani H, et al. Comparison of structure and catalytic performance of Pt-Co and Pt-Cu bimetallic catalysts supported on Al_2O_3 and CeO_2 synthesized by electron beam irradiation method for preferential CO oxidation. Int J Hydrogen Energy 2013;38:4456–65.
[20] Joint committee on powder diffraction standards; 1995.
[21] Ravel B, Newville M. ATHENA, ARTEMIS, HEPHAESTUS: data analysis for X-ray absorption spectroscopy using IFEFFIT. J Synchrotron Radiat 2005;12:537–41.
[22] Newville M. IFEFFIT: interactive EXAFS analysis and FEFF fitting. J Synchrotron Radiat 2001;8:322–4.
[23] Zabinski SI, Rehr JJ, Ankudinov A, Albers RC, Eller MJ. Multiple-scattering calculations of X-ray absorption spectra. Phys Rev B 1995;52:2995–3009.
[24] Komatsu T, Tamura A. Pt_3Co and PtCu intermetallic compounds: promising catalysts for preferential oxidation of CO in excess hydrogen. J Catal 2008;258:306–14.
[25] Kau LS, Spira-Solomon DJ, Penner-Hahn JE, Hodgson KO, Solomon EI. X-ray absorption edge determination of the oxidation state and coordination number of copper: application to the type 3 site in *Rhus vernicifera* Laccase and its reaction with oxygen. J Am Chem Soc 1987;109:6433–42.
[26] Penner-Hahn JE. Characterization of "spectroscopically quiet" metals in biology. Coord Chem Rev 2005;249:161–77.
[27] Ramallo-López JM, Lede EJ, Requejo FG, Rodriguez JA, Kim JY, Rosas-Salas R, et al. XANES characterization of extremely nanosized metal-carbonyl subspecies (Me = Cr, Mn, Fe, and Co) confined into the mesopores of MCM-41 materials. J Phys Chem B 2004;108:20005–10.
[28] Park PW, Ledford JS. The influence of surface structure on the catalytic activity of alumina supported copper oxide catalysts oxidation of carbon monoxide and methane. Appl Catal B Environ 1998;15:221–31.
[29] Centi G, Perathoner S. Nature of active species in copper-based catalysts and their chemistry of transformation of nitrogen oxides. Appl Catal A Gen 1995;132:179–259.
[30] Strohmeier BR, Leyden DE, Scott Field R, Hercules DM. Surface spectroscopic characterization of $Cu/A1_20_3$ catalysts. J Catal 1985;94:514–30.
[31] Wolberg A, Roth JF. Copper oxide supported on alumina III. X-ray K-absorption edge studies of the Cu^{2+} species. J Catal 1969;15:250–5.
[32] Shimizu K, Maeshima H, Yoshida H, Satsuma A, Hattori T. Spectroscopic characterization of $Cu\text{-}Al_2O_3$ catalysts for selective catalytic reduction of NO with propene. Phys Chem Chem Phys 2000;2:2435–9.
[33] Vila F, López Granados M, Ojeda M, Fierro JLG, Mariscal R. Glycerol hydrogenolysis to 1,2-propanediol with $Cu/\gamma Al_2O_3$: effect of the activation process. Catal Today 2012;187:122–8.
[34] Liu K, Wang A, Zhang T. Recent advances in preferential oxidation of CO reaction over platinum group metal catalysts. Am Chem Soc Catal 2012;2:1165–78.
[35] Shirley DA. High-resolution X-ray photoemission spectrum of the valence bands of gold. Phys Rev B 1972;5:4709–14.
[36] Ivanova AS, Slavinskaya EM, Gulyaev RV, Zaikovskii VI, Stonkus OA, Danilova IG, et al. Metal–support interactions in Pt/Al_2O_3 and Pd/Al_2O_3 catalysts for CO oxidation. Appl Catal B Environ 2010;97:57–71.